

## Rare isotope production in statistical multifragmentation

Scott Pratt, Wolfgang Bauer, Christopher Morling, and Patrick Underhill\*

*Department of Physics and Astronomy and National Superconducting Cyclotron Laboratory, Michigan State University,  
East Lansing, Michigan 48824*

(Received 22 September 2000; published 14 February 2001)

Producing rare isotopes through statistical multifragmentation is investigated using the Mekjian method for exact solutions of the canonical ensemble. Both the initial fragmentation and the sequential decay are modeled in such a way as to avoid Monte Carlo and thus provide yields for arbitrarily scarce fragments. The importance of sequential decay, exact particle-number conservation and the sensitivities to parameters such as density and temperature are explored. Recent measurements of isotope ratios from the fragmentation of different Sn isotopes are interpreted within this picture.

DOI: 10.1103/PhysRevC.63.034608

PACS number(s): 25.70.Pq, 24.10.Pa, 64.60.My

### I. INTRODUCTION

The study of rare isotopes is attracting increasing attention due to the recent development of radioactive beam facilities where isotopes are produced through nuclear collisions. Projectile and target nuclei might vary in size from a few dozen nucleons all the way to uranium. The mechanism for rare isotope production might entail the transfer of a few nucleons between the projectile and target, induced fission of the projectile, or at highest energy transfer, multifragmentation. This last mechanism, which assumes temperatures of a few MeV, is the focus of this study.

Multifragmentation is an extremely complicated process that takes place at a time scale of 100 fm/c. At such excitations tunneling through barriers plays a less central role than in fission. In this short time the system is able to sample an enormous number of configurations which makes dynamical calculations computationally very intensive. However, this very complexity lends justification to statistical calculations which have proven remarkably successful in predicting mass yields for excitation energies in the range of a few MeV per nucleon [1,2].

It is our aim to apply simple statistical calculations to the study of the production of rare isotopes, nuclei with neutron-to-proton ratios far from the valley of stability. Our investigation addresses a variety of questions.

(1) How do yields depend on the physical parameters of the thermalized system? Such parameters are size, overall neutron excess, density, and temperature.

(2) How sensitive are the yields with respect to various aspects of the modeling such as breakup density, level densities, and barrier penetration probabilities?

(3) Is there a qualitative and possibly quantitative explanation for the isospin amplification effects seen for light isotopes? Furthermore, do these effects carry over into the production of heavier or exotic isotopes? It has been experimentally observed that the ratio of mirror nuclei, e.g.,  $^{15}\text{O}/^{15}\text{N}$  or  $t/{}^3\text{He}$ , can be of order 10 even though the

neutron-to-proton ratio of the colliding nuclei is less than 1.5 [3].

(4) By dividing the ratio of isotope yields from the fragmentation of  $^{124}\text{Sn}$  by the same ratio from the fragmentation of  $^{112}\text{Sn}$ , one can extract the relative chemical potentials between the two systems which appears to be robust with respect to sequential decay. Can these results be quantitatively understood within the framework of a statistical model?

(5) Might multifragmentation provide a superior environment for the production of exotic isotopes in certain regions of the  $N/Z$  plane? Currently, abrasion/ablation models [4–6] provide the preferred scenario for creating rare isotopes and experiments have focused on searching for rare fragments at projectile rapidities. The EPAX parametrization [7], which is in common use for designing experiments, is built around such a picture. It is not clear to what degree multifragmentative pictures can either complement or compete with abrasion/ablation models.

The canonical ensemble is employed in this study. The motivation for choosing the canonical ensemble, along with descriptions of the statistical fragmentation algorithm and the sequential decay calculation, appear in the next section. Isotope yields are primarily determined by the breakup temperature and sequential decay. These themes are introduced in Sec. III. The importance of enforcing exact conservation of overall charge and baryon number with the canonical ensemble is discussed in Sec. IV. The sensitivity to the size and neutron excess of the overall system is explored in Sec. V while Sec. VI contains a study of the sensitivities to several aspects of the model such as breakup density, level density and tunneling through the Coulomb barrier during the sequential decay process. Recently, Xu *et al.* have measured yields of light fragments from the fragmentation of both  $^{112}\text{Sn}$  and  $^{124}\text{Sn}$ , and by taking ratios of isotope yields have determined the relative chemical potentials of the two systems [3]. This result is interpreted in Sec. VII. A summary is provided in Sec. VIII.

### II. MODELING STATISTICAL MULTIFRAGMENTATION AND THE SUBSEQUENT DECAY

The initial statistical fragmentation of the system is calculated assuming the canonical ensemble. The choice of the

\*Current address: Department of Physics, Washington University, Campus Box 1105, One Brookings Drive, St. Louis, MO 63130.

canonical ensemble is explained in the following subsection. The recursive method described in Sec. II B provides a probability for creating any state of any nuclide. The modeling of the subsequent sequential decay is described in Sec. II C.

### A. Choosing a statistical ensemble for fragmentation calculations

Statistical calculations have proven remarkably successful in describing mass yields for multifragmentative processes. Such models assume a fixed volume where all distributions of  $N$  neutrons and  $Z$  protons into various fragments and excited states are considered. A rather wide variety of thermal models have been employed in the study of nuclear fragmentation, including grand canonical [8], canonical [1], and microcanonical [2] treatments. Additionally, isospin effects have been studied in lattice-gas models [9–11] and in percolation [12,13]. Since our goal is to study the yields of rarely produced isotopes which may be produced in future radioactive beam facilities as rarely as in one per  $10^{17}$  events, we employ the methods recently promoted by Chase and Mekjian [14–16] which forego the need of using Monte Carlo methods. Majumder and Das Gupta have in fact studied boron, carbon, and nitrogen isotope production with a similar model to what is presented here [17]. The disadvantage of this method is that explicit interaction of fragments (beyond mean field or excluded volume effects) is outside the scope of the formalism.

Furthermore, we choose to focus on the canonical ensemble rather than the microcanonical ensemble which would strictly constrain the energy of the sampled configurations. The canonical distribution considers all configurations of the same net  $N$  and net  $Z$ , weighted by the Boltzmann factor  $e^{-\beta E}$ . The mean energy and variance of the energies are given by derivatives of the canonical distribution

$$\langle H \rangle = - \frac{\partial \ln(\Omega_c)}{\partial \beta} \quad (1)$$

$$\langle (H - \langle H \rangle)^2 \rangle = - \frac{\partial \langle H \rangle}{\partial \beta} \quad (2)$$

$$= T^2 \frac{\partial \langle H \rangle}{\partial T}. \quad (3)$$

It has been shown that these systems undergo first-order phase transitions, which implies an infinite specific heat for infinite systems. However, for systems of size  $A \approx 200$  the energy rises by approximately 4 MeV per nucleon as the temperature changes by one MeV in the range of  $T \approx 6$  MeV. This results in a variance of the energy per nucleon

$$\sigma_{E/A} \approx \frac{2T}{\sqrt{A}}. \quad (4)$$

Thus canonical calculations effectively sample configurations within an excitation energy window of approximately

1.0 MeV per nucleon, or less if the systems are much larger than  $A = 100$ , or if the temperature is away from the transition region.

Unless an experiment gates on excitation energies to an accuracy better than 1.0 MeV per nucleon, there is little motivation to pursue a microcanonical treatment. Microcanonical treatments have been shown to give much different results than canonical treatments in the study of fluctuations and fragment multiplicity distributions [16], topics which will not be pursued in this study.

Grand canonical treatments sum over configurations with different total  $Z$  and  $N$ . Since we are interested in the production of extremely neutron-rich or proton-rich fragments, it seems prudent to use the canonical ensemble. A comparison of grand canonical and canonical calculations is presented in Sec. IV.

### B. Fragmentation calculations with the canonical ensemble

Our calculations are based upon the recursion relations of Chase and Mekjian which permit one to sum over all partitions of the system into different nuclear fragments. The recursion relation for the canonical distribution function is

$$\Omega_{Z,N}(T) = \sum_c e^{-\beta E_c} = \sum_i \frac{a_i}{A} \omega_i(T) \Omega_{Z-z_i, N-n_i}(T), \quad (5)$$

where the label  $c$  in the summation in the first line indicates one particular configuration, and  $\omega_i$  is the partition function of a specific nuclear species  $i$ ,

$$\omega_i(T) = \frac{V_{\text{red}}(m_i T)^{3/2}}{(2\pi)^{3/2}} \sum_{\text{internal levels } j} e^{-\beta E_j}, \quad (6)$$

where  $m_i$  is the mass and  $z_i$ ,  $n_i$ , and  $a_i$  are the charge neutron number and baryon number of the species  $i$ . The reduced volume  $V_{\text{red}} = V_{\text{total}} - 2A/\rho_b$ , roughly accounts for the overlap of the nuclei. Given the default breakup density of one sixth  $\rho_0$ , the resulting reduced volume is four times the volume of a system at normal nuclear density.

Calculating the partition functions of specific species  $\omega_i$  is straightforward given the levels and degeneracies of the nuclei. This was done for all fragments with  $a < 6$ . However, many of the nuclei which are generated in this approach have not yet been observed, and for almost all of them the level structure is not known. Given our lack of understanding of the ground state energies, let alone the excited state energies, we employ a liquid-drop treatment. We have chosen the finite-range liquid-drop model (FRLDM) [18] as a means for generating ground state energies and have ignored the microscopic terms in the model which account for shell structure. The spectrum of excited states was generated by assuming a uniformly spaced assortment of single-particle states with spacing  $\Delta E = \alpha/\sqrt{A}$ , where  $\alpha$  is the level density parameter, chosen to be 10 MeV. The degeneracy of a state with excitation energy  $n\Delta E$  was found by counting all ways to arrange particles and holes such that they summed to the desired excitation energy. For heavy nuclei, the separation  $\Delta E$  becomes small, and when the separation fell below one

MeV, the spectrum is interpolated onto a mesh of 1.0 MeV resolution. Finally, all mass-formula energies were modified to account for screening of the Coulomb potential

$$E_{\text{Coul}} \rightarrow E_{\text{Coul}}(1 - \rho/\rho_0), \quad (7)$$

where  $\rho/\rho_0$  is the ratio of the density to nuclear matter density.

Once the functions  $\omega_i(T)$  were calculated, the partition function  $\Omega_{N,Z}(T)$  was then generated through the recursion relation, Eq. (5), in less than a second of computer time. Subsequently, the populations of individual levels  $j$  of a species  $i$  were found,

$$Y_{i,j} = \frac{d_{i,j} e^{-\beta E_{i,j}} \Omega_{Z-z_i, N-n_i}(T)}{\Omega_{Z,N}(T)}, \quad (8)$$

where  $E_{i,j}$  and  $d_{i,j}$  are the energy and degeneracy of the level.

### C. Modeling sequential decay

The vast majority of the nuclear levels considered in these calculations are particle-unstable, including the ground states of those species outside the proton and neutron drip lines. After the initial yields were calculated, the subsequent decay was modeled by apportioning the weight of an unstable level into all the levels into which the nucleus might decay. Eight decay modes were considered: proton, neutron, deuteron, dineutron, diproton,  $t$ ,  ${}^3\text{He}$ , and  $\alpha$ . The decay weights were chosen according to Weisskopf arguments. Considering the decay from a state  $i$  to a state  $f$  via the emission of particle of type  $k$  with energy  $E_k = E_f - E_i$ ,

$$\mathcal{R}_{i \rightarrow f}(E_k) \propto m E_k \sigma_{k,f \rightarrow i}, \quad (9)$$

where  $\sigma_{k,f \rightarrow i}$  is the capture cross section which we choose as the geometric cross section,  $\pi(R_f + R_k)^2$ , scaled by the Coulomb correction

$$\sigma_{k,f \rightarrow i} = \pi(R_f + R_k)^2 \frac{E_k - E_{\text{Coul}}}{E_k}. \quad (10)$$

Here,  $E_{\text{Coul}}$  is the Coulomb barrier

$$E_{\text{Coul}} = \frac{e^2 Z_f Z_k}{R_f + R_k}. \quad (11)$$

To account for particles tunneling through the Coulomb barrier, the  $s$ -wave contribution to tunneling through the barrier was estimated through the WKB approximation as

$$\begin{aligned} \sigma_s(E) &= \frac{\pi}{k^2} \exp \left\{ -2 \int_R^{r_0} \sqrt{\frac{2m}{\hbar^2} \left( \frac{Z_f Z_k e^2}{r} - E \right)} dr \right\}, \\ &= \frac{\pi}{k^2} \exp \left\{ -\frac{2\sqrt{2\mu} E r_0^2}{\hbar} \left[ \arctan \sqrt{\frac{r_0 - R}{R}} \right. \right. \\ &\quad \left. \left. - \frac{R}{r_0} \sqrt{\frac{r_0 - R}{R}} \right] \right\}, \\ r_0 &= \frac{Z_f Z_k e^2}{E}. \end{aligned} \quad (12)$$

If the energy exceeded the Coulomb barrier, the capture cross section was taken as  $\sigma_s = \pi/k^2$ . For all decays, both the classical form for the cross section in Eq. (10) and the  $s$  wave piece described above were compared and the larger of the two cross sections was chosen for the decay rates in Eq. (9).

Decays were calculated for all levels in all nuclei, beginning with the heaviest nuclei. For the decay of each level, the decay rate was calculated into every possible level energetically accessible through the eight decay modes listed previously. The weight associated with the decaying nucleus was then apportioned into all the states according to the rate for the decay into each state. The weights were also simultaneously added into the ground states of the eight nuclei representing the eight decay modes. Thus, the decaying process exactly preserved the initial  $N$  and  $Z$  of the original system. Given that heavier nuclei might have up to a thousand levels to decay with each level decaying into any of several hundreds of levels in a daughter nucleus, and given the existence of thousands of isotopes, the calculation of sequential decays often required a few hours.

### III. SENSITIVITY TO TEMPERATURE AND THE ROLE OF SEQUENTIAL DECAY

Fragmentation is clearly sensitive to temperature, not only in the mass yields but also in the isotopic yields. Higher temperatures allow the system to produce nuclei with unfavorable symmetry energies more efficiently. However, higher temperatures also result in hotter nuclei that experience longer decay chains which in turn push the resultant residues closer to the valley of stability. The interplay of temperature and symmetry energy is discussed in the following subsection by studying the liquid drop model. Section III B presents results of the canonical calculation with and without sequential decay. By modeling the fragmentation and decay of a system with  $A = 200$  and  $Z = 80$ , it is found that for lighter masses,  $a \approx 40$ , isotopes with highest  $n/a$  are best produced at temperatures near 5 MeV. Heavier neutron-rich fragments,  $a \approx 100$ , are best produced at lower temperatures near 3 MeV, but such production is certainly in the domain of fission, and purely statistical calculations should not be taken too seriously.

### A. Insights from the liquid-drop model

For a nuclear system at high excitation, where the initial nucleus is nearly completely dissolved into the constituent protons and neutrons, the neutron-to-proton ratio, and the triton-to- $^3\text{He}$  ratios are roughly equal to the neutron-to-proton ratio of the decaying nucleus. At lower excitation, where most of the mass resides in large nuclear fragments, this is no longer true. In heavy nuclei, the relative populations for nuclides of fixed  $a$  are determined by the symmetry energy, temperature, and Coulomb energy. Applying the grand canonical ensemble, one can make a liquid-drop estimate of the relative populations given the chemical potential  $\mu_I \equiv (\mu_n - \mu_p)/2$ , related to the difference in neutron and proton number

$$P_a(n-z) \propto \exp\left\{ \left( -\xi(n-z)^2/a - b_c \left[ \frac{a+(z-n)}{2} \right]^2 \right) / a^{1/3} + \mu_I(n-z) \right\} / T, \quad (13)$$

where  $\xi$  is the symmetry term in the liquid-drop model. The Coulomb term also contributes to the symmetry energy. The parameters chosen here are  $b_c = 0.7$  MeV and  $\xi = 23.4$  MeV. A more complicated parameter set is employed in the FRLDM. However, for illustrative purposes, we consider the Bethe-Weizsäcker liquid-drop model here.

Ignoring the Coulomb term and completing the square in the exponential above allows calculation of the mean neutron excess for fragments of mass  $a$ :

$$\langle n-z \rangle = a \frac{\mu_I}{2\xi}. \quad (14)$$

The neutron to proton ratio is then

$$\frac{Y_n}{Y_p} = \exp(2\mu_I/T) = \exp\left(4\frac{\xi}{T} \frac{\langle n-z \rangle}{a}\right). \quad (15)$$

If most nucleons reside in large fragments, the ratio  $\langle n-z \rangle/a$  of a single species equals the ratio for the entire system.

By considering the limit where  $\langle n-z \rangle/a$  is small, one can derive the isospin amplification factor

$$\frac{Y_n - Y_p}{Y_n + Y_p} = \tanh \mu_I/T \quad (16)$$

$$\approx 2\frac{\xi}{T} \frac{\langle n-z \rangle}{a}. \quad (17)$$

Thus, the isospin amplification factor is  $2\xi/T$ , which exceeds 10 for temperatures less than 5 MeV. This ratio is the same for all mirror nuclei related by changing one proton to one neutron, e.g.,  $t$ - $^3\text{He}$  and  $^{15}\text{O}$ - $^{15}\text{N}$ . Large ratios of mirror nuclei have been observed in intermediate-energy heavy ion collisions [3]. It should be noted that Serot and Müller posulated similar ideas regarding isospin fractionation in terms

of phase separation [19] and that Samaddar and Das Gupta have made similar conclusions using the lattice gas model [10].

The distribution described in Eq. (13) can be described by an offset and a Gaussian width. The offset is largely determined by the neutron fraction  $N/A$  of the composite system and does not depend strongly on the temperature unless the temperature becomes so high that protons, neutrons, tritons, and  $^3\text{He}$  fragments can absorb much of any initial excess of the neutron number. The width depends on the ratio of symmetry energy to the temperature:

$$\sigma_{n-z} = \sqrt{\frac{Ta}{2\xi}}. \quad (18)$$

Thus, although the ratio of yields of mirror nuclei tend to be largest for lower temperatures, higher temperatures result in the broadest widths and the greatest yields for nuclei with extreme neutron or proton imbalances. However, this conclusion will be significantly modified by sequential decay.

### B. Results for the fragmentation of $A=200$ , $Z=80$ nuclei

In this section we present results from the calculations described in Sec. II which combine the canonical ensemble with sequential decay. We will see that the expectations from the previous section, that higher temperatures produce more isotopes far away from the valley of stability, are qualitatively modified by the effects of sequential decay. Sequential decay will more strongly narrow the distribution when the temperature is higher and more decays occur, allowing the final residue to approach the valley of stability more closely. Combined with the production probability of producing a fragment of size  $a$  with any  $n-z$ , the optimum temperature for producing fragments with a large neutron excess is not trivially understood.

Figure 1 displays the yield of  $a=40$  fragments as a function of  $n-z$  for the fragmentation of an  $A=200$ ,  $Z=80$  system at several temperatures. The upper panel displays yields for the case where sequential decay is neglected. Clearly, higher temperatures create the best conditions for creating highly neutron-rich nuclei when sequential decay is neglected. The  $T=4.5$  MeV results are well described by the Gaussian resulting from the liquid-drop expression, Eq. (13). The magnitude and center of the Gaussian were adjusted to fit the peak but the width was determined by the liquid-drop parameters.

Post-decay yields are displayed in the lower panel of Fig. 1. Sequential decay strongly narrows the distribution, especially for higher temperatures. Figure 2 displays the yields of sulphur isotopes for the same system. From Figs. 1 and 2, one concludes that the probability of producing rare neutron-rich isotopes is highest for temperatures near 5 MeV for mass  $a \approx 40$  fragments.

Yields of  $a=100$  fragments are shown in Fig. 3. Since heavier fragments evaporate more particles, they are more affected by sequential decay. For heavier fragments, especially at temperatures less than 3 MeV, fission should provide the dominant production mechanism. Although the sta-

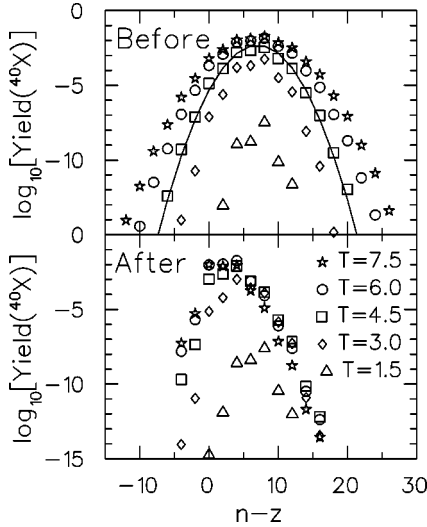


FIG. 1. Yields of mass 40 fragments are shown for the fragmentation of an  $A=200$ ,  $Z=80$  system at a variety of temperatures. Yields are shown both for the case where sequential decay is included (lower panel) and neglected (upper panel). The pre-decay yields at 4.5 MeV are well described by a Gaussian (line) where the width is determined by liquid drop parameters described in Eq. (13). Pre-decay yield curves are broadest for higher temperatures, but post-decay yields of very neutron rich fragments are largest for temperatures near 5 MeV.

tistical description presented here does consider fissionlike partitions of the system, both dynamics and shell structure play a significant role in fragmentation at low excitation where barriers play a pivotal role. For that reason, we confine our future discussion to the production of lighter fragments  $a < A/3$ .

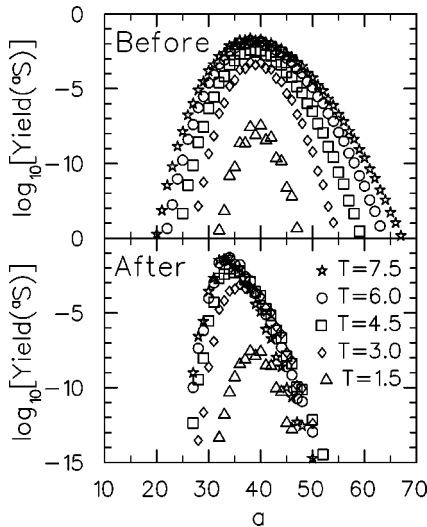


FIG. 2. Sulphur yields from the fragmentation of an  $A=200$ ,  $Z=80$  system are displayed for a variety of temperatures. Yields are shown both for the case where sequential decay is included (lower panel) and neglected (upper panel). As in Fig. 1 the best chance of producing isotopes near the neutron drop line occurs for temperatures near 5 MeV.

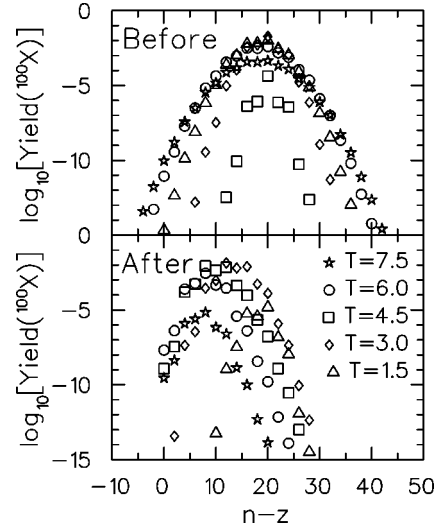


FIG. 3. The same as Fig. 1, except for mass 100 fragments. Post-decay yields for extremely neutron-rich fragments in this mass range are largest for temperatures near 3 MeV.

#### IV. GRAND CANONICAL vs CANONICAL ENSEMBLES

The canonical ensembles employed in this study enforce exact conservation of neutron and proton number. In order to understand the importance of this constraint, we present corresponding calculations in the grand canonical ensemble. In the grand canonical ensemble densities are determined by chemical potentials, and the presence of a fragment of type  $i$  does not affect the possibility of observing a second fragment. A grand canonical ensemble supposes either an infinite system or one chemically connected to an infinite bath of both heat and particles.

Performing calculations in the grand canonical ensemble begins, as in the canonical ensemble, by calculating partition functions as defined in in Eq. (6). The yield of fragments of type  $i$  is then

$$Y_i = \omega_i(T) e^{\mu_n n_i / T + \mu_p z_i / T}. \tag{19}$$

One must then find the chemical potentials  $\mu_p$  and  $\mu_n$  that give the desired net neutron and proton numbers. In practice, this is accomplished numerically by applying Newton's method. For the results presented here, only nuclei of mass and charge less than that of the entire system were included in the sum. Neglecting higher masses only affects results at low temperatures.

Yields of  $a=40$  fragments from grand canonical and canonical calculations are presented in Fig. 4 for the fragmentation of an  $A=200$ ,  $Z=80$  system, and a system of half that size, and are compared to results using the grand canonical ensemble. The yields are similar for the two ensembles when considering fragmentation of the heavier system, but are significantly different for the lighter example. The reduced production of extremely neutron-rich nuclei from the fragmentation of the  $A=100$  system is easily understood as resulting from the absolute conservation of neutron number. In summary, use of the grand canonical ensemble is invalid for

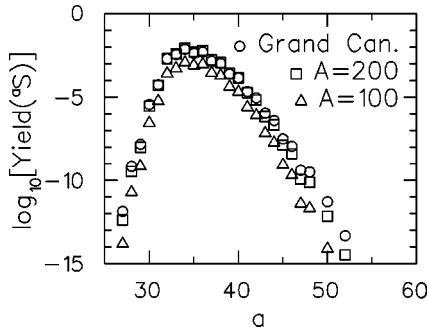


FIG. 4. The importance of enforcing baryon number and charge conservation in the statistical treatment is illustrated by comparing yields of sulphur isotopes for canonical and grand canonical calculations. As expected, fragmentation of the  $A=200$ ,  $Z=80$  system is better described by the grand canonical calculation than fragmentation of the lighter system  $A=100$ ,  $Z=40$ .

smaller systems, and even in the case of large systems, can result in overpredicting yields by an order of magnitude near the neutron drip lines.

### V. ISOTOPE PRODUCTION AS A FUNCTION OF SYSTEM SIZE AND CHARGE

By fragmenting heavier systems, one is able to create hot systems with higher neutron fractions. By choosing larger systems, yields are less affected by the constraints of exactly conserving the net number of neutrons and protons. Although the qualitative trend is clear—larger and more neutron-rich systems are better suited to producing extremely neutron-rich fragments—quantitative dependencies might be rather surprising given the amplifications mentioned earlier.

Yields for sulphur fragments are shown in Fig. 5 for three systems ( $A=200$ ,  $Z=80$ ), ( $A=200$ ,  $Z=85$ ), and ( $A=100$ ,  $Z=40$ ). Each system is chosen to fragment at a temperature of 4.5 MeV. The importance of beginning with the most neutron-rich system is clearly apparent in the comparison of the  $Z=80$  and the  $Z=85$  cases. Here, the neutron fraction changes from 0.6 to 0.575. Furthermore, comparison with the smaller system at the same neutron fraction  $N/A=0.6$  demonstrates the modest enhancement of neutron-rich fragments involved in using larger systems.

Given the sensitivity of the yields to changing the neutron and proton number of the fragmenting system, evaporation of neutrons during the early stages of the reaction should significantly reduce the production of rare neutron-rich isotopes. During the first 100 fm/c, Weisskopf arguments suggest that 20 to 30 neutrons, but only 5 to 10 protons, might evaporate from a uranium nucleus heated to a temperature of 10 MeV. The neutron fraction of the residue might thus change from 0.614 to  $\approx 0.59$  during the evaporation which significantly reduces the possibility to emit fragments near the neutron drip line. Fission yields are also affected by the number of evaporated pre-fission neutrons, which can be sizable, especially when the fission time scale is large.

If one wishes to find reactions with the highest abundances of rare neutron-rich fragments, one should try to minimize the number of neutrons emitted in the prefragmen-

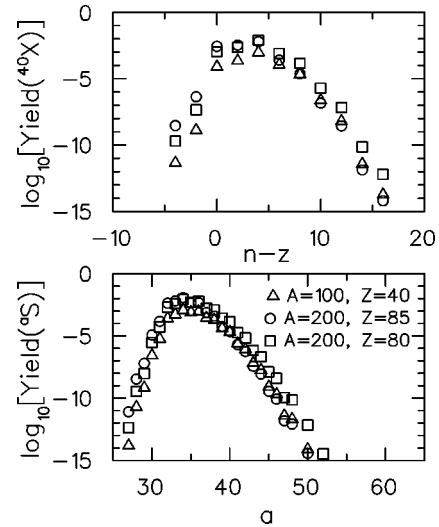


FIG. 5. Yields of mass 40 fragments (upper panel) and sulphur isotopes (lower panel) are shown for a variety of systems fragmenting at a temperature of 4.5 MeV. Yields of neutron-rich isotopes were moderately decreased when considering a smaller overall system of the same neutron fraction. For the  $A=200$  systems yields were substantially reduced by lowering the net number of neutrons from 120 to 115.

tation stage of the collision. Reducing the number of neutrons emitted during the prefragmentation stage might be accomplished by choosing heavy-ion collisions as a means of producing multifragmented systems. Since heavy ion collisions, especially midcentral collisions, retain some of the initial collective longitudinal motion of the beam, the expansion does not require as much time to accelerate from rest as it would in a  $pA$  collision. Furthermore, by colliding two very heavy nuclei, the global system would be relatively proton rich and not emit neutrons as preferentially, relative to protons, during the early stages of the collision. In fact, the midrapidity region, often referred to as the neck, might be even more neutron rich than the target or projectile [20]. Of course, the disadvantage to using heavy-ion collisions is that lower beam energies are used and the produced fragments are not as forward focused which might make them more difficult to detect. If one wishes to produce fragments with charges greater than calcium,  $z=20$ , and energies less than  $30a$  MeV, electron recombination and the resulting impure charge states makes detection and refocusing especially difficult.

### VI. SENSITIVITY TO BREAKUP DENSITY, LEVEL DENSITY, AND SUB-BARRIER EVAPORATION

Although the calculated yields of rare fragments depend on details of the modeling procedure, it is not obvious to what degree yields are sensitive to particular aspects of the modeling. One obvious parameter is the symmetry energy parameter. As the symmetry energy is uncertain by one or two MeV outside the region of measured nuclei the associated Boltzmann factors might change by a factor of 2. Clearly, a lower symmetry energy will lead to broader isotope distributions. The sensitivity to other aspects of the

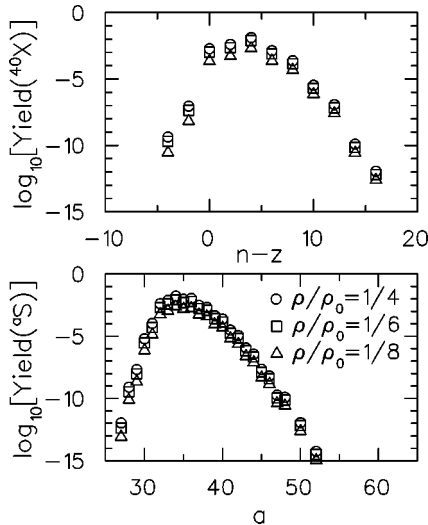


FIG. 6. Fragmentation of an  $A=200$ ,  $Z=80$  system at a temperature of 4.5 MeV is calculated for three different breakup densities. Yields are shown for mass 40 fragments as a function of  $n-z$  (upper panel) and for sulphur fragments as a function of mass (lower panel). The breakup density affects the mass distribution more strongly than the relative probabilities for isotopes of fixed mass.

modeling is not so trivial. In this section we consider three sources of uncertainty: the breakup density, the level density parameter, and sub-barrier evaporation.

Adjusting the breakup density affects the mass distributions as larger breakup volumes lead to preferential emission of many small fragments. To determine the sensitivity of the isospin distributions to the breakup density, the fragmentation of an  $A=200$ ,  $Z=80$  system was considered at three breakup densities  $\rho_0/8$ , the default breakup density  $\rho_0/6$ , and  $\rho_0/4$ . The yield of fragments of mass  $a=40$  and of sulphur isotopes are displayed in Fig. 6 assuming a breakup temperature of 4.5 MeV. The distributions of isotopes of fixed mass are fairly insensitive to the choice of breakup density. This is not surprising given the liquid-drop arguments presented in Sec. III A. The distribution of sulphur isotopes is broader for the higher breakup densities as would be expected since higher densities lead to increased production of heavier fragments.

The level density parameter affects results with regards to the initial population of isotopes, the relative populations of levels of a given isotope, and in the dynamics of the sequential decay. The breakup of an  $A=200$ ,  $Z=80$  system is again considered, and the yields of mass 40 fragments and sulphur isotopes are displayed in Fig. 7 for three level density parameters 8 MeV, the default value of 10 MeV, and 12 MeV. The distributions are noticeably broader for the higher level density parameters. Very little effect was evident in the pre-decay yields and thus this sensitivity derives from the dynamics of the sequential decay. This suggests the importance of improving how excited states are generated as the level density is known to have a strong dependence on shell structure.

The final aspect of the modeling considered here is barrier penetration, which plays an important role in sequential de-

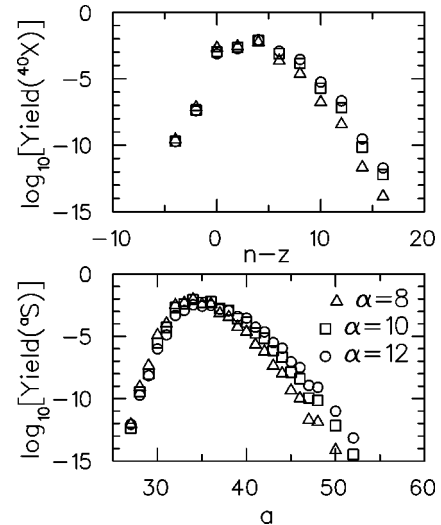


FIG. 7. The yields of mass 40 isotopes (upper panel) and sulphur isotopes (lower panel) are shown to be sensitive to the choice of level density parameter  $\alpha$ . Higher level density parameters lead to broader isotope distributions due to the dynamics of sequential decay. Again, calculations concerned an  $A=200$ ,  $Z=80$  system at a temperature of 4.5 MeV.

ca. Sequential decay, as seen in Figs. 1 and 2, strongly narrows the isotope distributions as evaporation pushes the fragments towards the valley of stability. The Coulomb barrier also leads to preferential emission of neutrons relative to protons. In our calculations a fixed Coulomb barrier was imposed with an additional consideration of  $s$ -wave tunneling. To understand the importance of tunneling, calculations were performed with and without tunneling. Calculations were also performed with the Coulomb barrier completely absent. Results considering the fragmentation of the  $A=200$ ,  $Z=80$  system at a temperature of 4.5 MeV are displayed in Fig. 8. Ignoring the tunneling increased the yields of proton-rich fragments but left the yield of neutron-rich fragments unchanged. Ignoring the Coulomb barrier altogether significantly reduced the population of proton-rich fragments and only slightly increased the yield of neutron-rich fragments.

Interpretation of Fig. 8 suggests that the yield of neutron-rich fragments is surprisingly insensitive to the imposition of the Coulomb barrier as the preference of emitting neutrons to protons is more strongly derived from the greater phase space available when decaying towards the valley of stability. However, if one were interested in the production of proton-rich fragments, there would be a strong motivation to improve the treatment of the Coulomb barrier.

## VII. ISOSPIN AMPLIFICATION AND BARYONIC CHEMICAL POTENTIALS

The phenomenon of isospin amplification was presented in Sec. III A in the context of the liquid drop model and was also discussed in Sec. V. It was seen that relatively small neutron excesses could result in large increases in the yields of neutron-rich isotopes. Experimentally, it has been observed that yields are indeed quite sensitive to the neutron fraction of the fragmenting system. By creating a ratio of

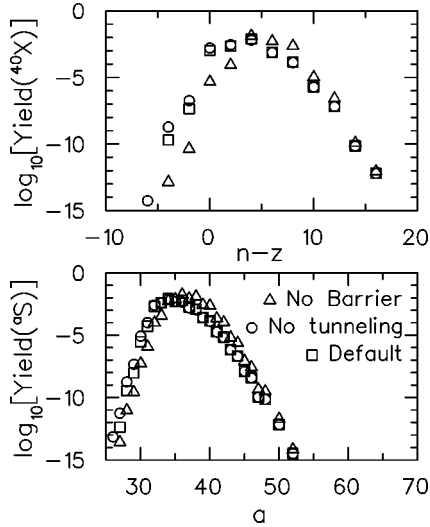


FIG. 8. The sensitivity of isotope yields to details of evaporation criteria are studied by considering the yields of sulphur isotopes from the fragmentation of an  $A=200$ ,  $Z=80$  system at a temperature of 4.5 MeV. Results from three cases are displayed. The evaporative description in the default calculation (squares) assumes a Coulomb barrier with an  $s$ -wave tunneling contribution described in Eq. (12). Calculations were repeated with no tunneling (diamonds) and with the barrier eliminated (triangles), making the emission of neutrons and protons equal. Yields near the neutron drip line were insensitive to details of barrier, but yields near the proton drip line were indeed sensitive to the barrier and to the tunneling.

yields for different isotopes from the fragmentation of  $^{112}\text{Sn}$  and dividing by the same ratio for the fragmentation of  $^{124}\text{Sn}$ , one is able to extract the difference of the chemical potential for the two fragmenting systems.

To better explain the ratio, one considers the population of a level  $i$  of an isotope of mass  $a$  in the grand canonical ensemble

$$Y(^aX) = \sum_i V(2J_i + 1) \left( \frac{amT}{2\pi} \right)^{3/2} \times \exp \left\{ \frac{-B_i + z\mu_p + (a-z)\mu_n}{T} \right\}. \quad (20)$$

From the results of the previous sections, it is clear that the yield is significantly affected by sequential decay. However, studies using the MMC model [21,3] have revealed a surprising insensitivity of the following ratio to sequential decay:

$$\mathcal{R}_{112}^{124(a)C/^{12}C} = \frac{Y^{124(a)C}/Y^{124(^{12}C)}}{Y^{112(a)C}/Y^{112(^{12}C)}}, \quad (21)$$

where the 124 and 112 refer to the different isotopes of the overall system. This ratio should yield  $e^{(n-z)\Delta\mu_n/T}$ , where  $\Delta\mu_n$  is the difference of the neutron chemical potentials of

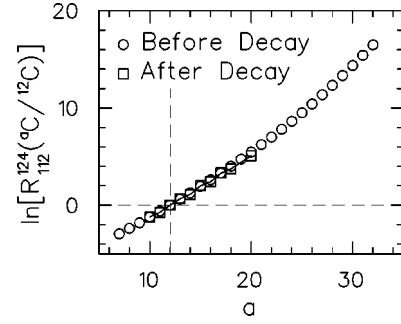


FIG. 9. Ratios of carbon isotope yields for the fragmentation of  $^{124}\text{Sn}$  are divided by the same ratios for the fragmentation of  $^{112}\text{Sn}$  to obtain a quantity which should reflect  $\exp\{(n-z)\Delta\mu_n/T\}$ , where  $\Delta\mu_n$  is the increase of the neutron chemical potential resulting from using a heavier tin isotope. The logarithm of that ratio, which is presented here, rises linearly with  $a$  as expected. The pre-decay results (squares) and the post-decay results (squares) are remarkably similar.

the  $A=124$  and  $A=112$  systems. By creating a similar ratio using isotopes of the same neutron number, one is able to extract  $\Delta\mu_p$ .

To illustrate the insensitivity of the ratio to sequential decay, the logarithm of the ratio is shown both before and after sequential decay in Fig. 9 for the fragmenting  $^{112}\text{Sn}$  and  $^{124}\text{Sn}$  systems at a temperature of 4.5 MeV. The slight non-linearity of the pre-decay results derives from the finite size of the system, i.e., a grand canonical calculation would yield a straight line.

The resulting ratio also clearly depends on temperature and breakup density. To illustrate the temperature dependence, calculations were performed for three temperatures 3.0, 4.5, and 6.0 MeV. The logarithm of the ratio was in this case multiplied by the temperature so that one could focus on  $\Delta\mu$  rather than  $\Delta\mu/T$ . The slopes weakly depend on the temperature as shown in the lower panel of Fig. 10. The sensitivity to the breakup density was also investigated and found to be rather weak.

The upper panel of Fig. 10 displays a line derived from analysis of several experimentally measured isotope ratios [3], where the ratios were observed to be surprisingly robust with respect to the choice of element and isotopes. The comparison with data is difficult to interpret. At the time in a collision where multifragmentation occurs, one would expect some of the extra neutrons in the  $^{124}\text{Sn}$  system to have boiled off. Thus, it is not surprising that the calculation overpredicts  $\Delta\mu_n$  as the calculation assumes the systems differ by 12 neutrons. The experimental result was also of a different effective size due to the fact that the mechanism for excitation was semiperipheral heavy ion collisions. As the experiment involved  $^{124}\text{Sn} + ^{124}\text{Sn}$ ,  $^{112}\text{Sn} + ^{124}\text{Sn}$ , and  $^{112}\text{Sn} + ^{112}\text{Sn}$  collisions, the effective system size might have been either more or less than the size of a single Sn ion depending on the centrality of the collision and experimental acceptance. Nonetheless, several positive conclusions should be drawn from this analysis. First, the ratios are indeed robustly independent of sequential decay, even when one considers isotopes far along the isotope chain from stability. Secondly, the experimental results would seem to be consistent with model

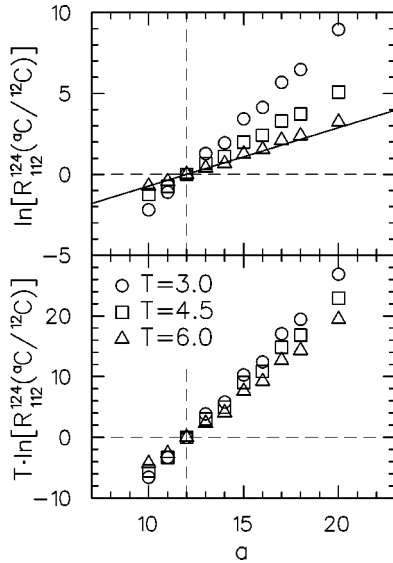


FIG. 10. In the top panel the same quantity as in Fig. 9 is displayed for calculations at three temperatures 3.0, 4.5, and 6.0 MeV. The solid line represents the experimentally extracted value of  $\Delta\mu_n$  from Ref. [3]. The consistency of the experimental results with the  $T=3$  MeV results may be misleading as the calculations ignored the fact that some of the extra neutrons associated with  $^{124}\text{Sn}$  could have evaporated before the onset of multifragmentation. The same results are displayed in the lower panel, only multiplied by the temperature. This illustrates that  $\Delta\mu_n$  is fairly insensitive to the temperature.

predictions if one were to assume that approximately a third of the extra neutrons gained from going from  $^{112}\text{Sn}$  to  $^{124}\text{Sn}$  evaporated prior to multifragmentation.

### VIII. SUMMARY AND CONCLUSIONS

Statistical multifragmentation has been investigated in regards to the production of rare nuclides, particularly neutron-rich isotopes. Statistical calculations have been performed in the canonical ensemble, taking into account exact conservation of  $N$  and  $Z$ . By comparing to calculations in the grand canonical ensemble, particle-number constraints were seen to be non-negligible, especially for the fragmentation of smaller systems. Assuming a simple liquid-drop form for the ground-state energies and assuming a simplified form for the distribution and degeneracies of excited states, initial yields were calculated for every level of every possible isotope. Sequential evaporation has been modeled by calculating the ways to partition the initial weight of every particle-unstable level into any state to which it might decay. Eight modes of decay were considered. Since neither the calculation of the initial distribution nor the modeling of the sequential decay involved Monte Carlo procedures, it was possible to calculate yields for extremely rare isotopes.

By considering yields of fragments of a fixed  $a$  as a function of  $n-z$ , two lessons were learned by considering a simple liquid drop model. First, the width of the initial distribution was determined largely by the ratio of the tempera-

ture to the symmetry term in the liquid-drop model. Secondly, isospin amplification, or isospin fractionation, could also be simply understood in terms of the same two quantities.

Sequential decay dramatically altered the yields, pushing the yields towards the valley of stability. The effects were strongest for larger fragments and for higher temperatures. As the initial distributions for fragments of fixed  $a$  as a function of  $n-z$  were broadest at high temperature, inclusion of sequential decay shows that 5 MeV is the best temperature for creating rare neutron-rich fragments in the  $a=40$  region. For heavy fragments with  $a=100$ , the optimum temperature was near three MeV which is more in the domain of fission than the domain of multifragmentation.

In order to understand the sensitivity of the calculations to various aspects of the modeling, the breakup density, level density, system size, and system neutron fraction were systematically varied. Results were weakly dependent on the breakup density and moderately sensitive to the level density. Larger systems lead to somewhat broader yields due to finite-size constraints. Yields were especially sensitive to small changes in the isospin composition of the overall system. Thus, choosing projectiles and targets with large neutron fractions, e.g.,  $N/A$  for uranium is 0.614 and  $N/A$  for  $^{124}\text{Sn}$  is 0.597, strongly increases the chances of creating isotopes near the neutron drip line. Finally, the sensitivity of the yields with respect to details of the evaporation was considered by adjusting the Coulomb barrier that leads to preferential emission of neutrons as opposed to protons. The yields of neutron-rich fragments were surprisingly insensitive to the barrier and changed almost imperceptibly when the Coulomb barrier was removed altogether. Proton-rich fragments were, however, quite sensitive to the details, as the tunneling allowed proton-rich fragments to return to the valley of stability.

The ability of statistical models to explain isotope production is certainly of scientific interest in its own right. Additionally, one might also consider whether multifragmentation could offer a competitive means for creating rare isotopes. However, separating and focusing particles could be problematic. If one fragmented heavy nuclei, which have the broadest yields, the Coulomb forces between the fragment of interest and various parts of the residual system would spread the emission over a large kinematic region making separation or focusing of the produced particles difficult. This would be especially true for fragments produced at midrapidity. Thus, it is difficult to discern whether there is a pragmatic side to the isospin degree of freedom in multifragmentation. To date, experiments that measure isotope yields have either been designed to focus on projectile rapidities and thus ignore multifragmentative events, or have measured production of light elements  $a < 20$ . If statistical descriptions are shown to accurately describe isotope production for a broader range of nuclides, it might warrant serious consideration of designing an apparatus to capture and identify very rare isotopes in a very different environment than projectile fragmentation.

## ACKNOWLEDGMENTS

This work was supported by the National Science Foundation, Grants No. PHY-96-05207 and PHY-00-70818. Patrick Underhill was supported by the Research Experience for Undergraduates program at Michigan State University

which is sponsored by the National Science Foundation, Grant No. PHY-94-24140. C.M. was supported by the Undergraduate Professorial Assistants Program at Michigan State University. W.B. acknowledges support from the Alexander-von-Humboldt Foundation.

- 
- [1] J. P. Bondorf, A. S. Botvina, A. S. Iljinov, I. N. Mishustin, and K. Sneppen, *Phys. Rep.* **257**, 133 (1995).
  - [2] D. H. E. Gross, *Rep. Prog. Phys.* **53**, 605 (1990); D. H. E. Gross, *Phys. Rep.* **279**, 119 (1997).
  - [3] H. S. Xu *et al.*, *Phys. Rev. Lett.* **85**, 716 (1999).
  - [4] W. Wlazlo *et al.*, LANL Report No. nucl-ex/0002011.
  - [5] J. Cugnon, C. Volant, and S. Vuillier, *Nucl. Phys.* **A620**, 457 (1997).
  - [6] R. E. Prael and H. Lichtenstein, Los Alamos Report No. UR-89-3014, 1989.
  - [7] K. Sümmerer and B. Blank, LANL Report No. nucl-ex/9911006.
  - [8] G. Fai and J. Randrup, *Nucl. Phys.* **A404**, 551 (1983).
  - [9] J. Pan, S. Das Gupta, and M. Grant, *Phys. Rev. C* **57**, 1839 (1998).
  - [10] S. K. Samaddar and S. Das Gupta, *Phys. Rev. C* **61**, 034610 (2000).
  - [11] Ph. Chomaz and F. Gulminelli, *Phys. Lett. B* **447**, 221 (1999).
  - [12] G. Kortemeyer, W. Bauer, and G. J. Kunde, *Phys. Rev. C* **55**, 2730 (1997).
  - [13] H. M. Harreis and W. Bauer, LANL Report No. cond-mat/9907330; *Phys. Rev. B* **62**, 8719 (2000).
  - [14] K. C. Chase and A. Z. Mekjian, *Phys. Rev. C* **52**, R2339 (1995); **50**, 2078 (1994); **49**, 2164 (1994).
  - [15] S. Das Gupta and A. Z. Mekjian, *Phys. Rev. C* **57**, 1361 (1998); P. Bhattacharyya, S. Das Gupta, and A. Z. Mekjian, *ibid.* **60**, 064625 (1999).
  - [16] S. Pratt and S. Das Gupta, *Phys. Rev. C* **62**, 044603 (2000).
  - [17] A. Majumder and S. Das Gupta, *Phys. Rev. C* **61**, 034603 (2000).
  - [18] P. Möller, J. R. Nix, W. D. Myers, and W. J. Swiatecki, *At. Data Nucl. Data Tables* **59**, 185 (1995).
  - [19] H. Müller and B. D. Serot, *Phys. Rev. C* **52**, 2072 (1995).
  - [20] E. Plagnol *et al.*, *Phys. Rev. C* **61**, 014606 (2000).
  - [21] A. S. Botvina *et al.*, *Phys. Lett. B* **416**, 56 (1998).